Science Advances
AAAS

advances.sciencemag.org/cgi/content/full/6/10/eaaw7853/DC1

Supplementary Materials for

Mapping the structure and biological functions within mesenchymal bodies using microfluidics

Sébastien Sart, Raphaël F.-X. Tomasi, Antoine Barizien, Gabriel Amselem, Ana Cumano, Charles N. Baroud*

*Corresponding author. Email: charles.baroud@pasteur.fr

Published 4 March 2020, *Sci. Adv.* **6**, eaaw7853 (2020)
DOI: 10.1126/sciadv.aaw7853

The PDF file includes:

Other Supplementary Material for this manuscript includes the following:

(available at advances.sciencemag.org/cgi/content/full/6/10/eaaw7853/DC1)

Table S1. Flow rate for cell loading and phase exchange.

Step	Liquid loader	Flow rate (μl/min)	Approximate delivered volume (μL)
Cell loading	Chamber	50	150
	Junction	13	40
	Cells	8 - 8.4	25
Surfactant washing	Exit of the chamber	80	2000
Culture medium	Exit of the chamber	4	100

Table S2. Primer sequences.

Gene	Orientation	Sequence	Product size (bp)	Tm (°C)
TSG-6	Forward	AAGCACGGTCTGGCAAATACAAGC	139	60
	Reverse	ATCCATCCAGCAGCACAGACATGA		
Cox-2	Forward	ACTCTGGCTAGACAGCGTAA	145	60
	Reverse	ACCGTAGATGCTCAGGGAC		
STC-1	Forward	GCTTAAAATGCATCGCCAAC	273	60
	Reverse	TTTTCTCCATCAGGCTGTCTC		
VEGF-A	Forward	GCACCCATGGCAGAAGG	90	60
	Reverse	CTCGATTGGATGGCAGTAGCT		
RUNX-2	Forward	AGATGATGACACTGCCACCTCTG	125	60
	Reverse	GGGATGAAATGCTTGGGAACT		
CEBP/α	Forward	GAGGGACCGGAGTTATGACA	130	60
	Reverse	TGGTGGTTTAGCAGAGACGC		
SOX-9	Forward	CATGAGCGAGGTGCACTCC	112	60
	Reverse	TCGCTTCAGGTCAGCCTTG		
GADPH	Reverse	CTCGATTGGATGGCAGTAGCT	207	60
	Forward	TGATGACATCAAGAAGGTGGTG		

Table S3. Small molecules for the inhibition of molecular pathways regulating hMSC behavior; the concentrations used in this study are adapted from (*59*, *60*).

Small molecule	Manufacturer	Target	Inhibited molecular signaling	Concentration used in this study
Indomethacin	Sigma-Aldrich	COXs	COX-2	10 μM (PGE-2 ELISA) or 25 μM (VEGF-A ELISA)
DAPT	Sigma-Aldrich	γ-secretase	Notch	50 μM
QNZ	Sigma-Aldrich	NF-κB transcriptional activation	NF-κB	10 μM
Cytochalasin D	Sigma-Aldrich	Actin monomers	Actin polymerization	1 μM
Y-27632	Sigma-Aldrich	ROCK	Formation of stress fibers	10 μM

Table S4. Statistical tests and *P* values.

Figure number	Assumptions	Statistical test	P-values
Fig. 3D	Normality, independent sample values, equal variances	Two-sample t-test	r/R between 0 and 0.2, p < 1e-4 ; r/R= 0.3 and r/R = 0.4, p < 0.01; r/R = 0.35, p = 0.51; r/R = 0.4, p = 0.22
Fig. 3G	Normality, independent sample values, equal variances	Two-sample t-test	RUNX2: $CD146^{dim}$ vs $CD146^{bright}$=0.02
Fig. 4D	Normality, independent sample values, equal variances, multiple comparisons	ANOVA, parametric posthoc procedure with Sidak's correction	1 vs 2: p < 1e-4; 2 vs 3: p < 1e-4; 3 vs 4: p < 1e-4; 4 vs 5: p < 1e-4; 5 vs 6: p < 1e-4; 6 vs 7: p < 1e-4; 7 vs 8: p = 1.0000
Fig. 5A	Normality, independent sample values, equal variances	Two-sample t-test	TSG-6: p = 0.0002; COX-2: p = 0.0043; STC-1; p = 0.0012 VEGF; p=0.04
Fig. 5C	Normality, independent sample values, equal variances, multiple comparisons	ANOVA, posthoc procedure with Sidak's correction	a. PEG2: 2D vs 3D: p = 0.001; 3D vs 3D+COX inh: p = 0.03 b. VEGF: 2D vs 3D: < 1e-4; 3D vs 3D+COX inh: p < 1e-4
Fig. 5E	Normality, independent sample values, equal variances, multiple comparisons	ANOVA, parametric posthoc procedure with Sidak's correction	1 vs 2: p < 1e-4; 2 vs 3: p < 1e-4; 3 vs 4: p < 1e-4; 4 vs 5: p < 1e-4; 5 vs 6: p < 1e-4; 6 vs 7: p = 0.4930; 7 vs 8: p = 1.0000
Fig. 5F	Normality, independent sample values, equal variances, multiple comparisons	ANOVA, parametric posthoc procedure with Sidak's correction	1 vs 2: p < 1e-4; 2 vs 3: p < 1e-4; 3 vs 4: p < 1e-4; 4 vs 5: p < 1e-4; 5 vs 6: p < 1e-4;
Fig. 6B	Independent sample values, known reference	One-sample sign test	QNZ: p < 1e-4 ; DAPT: p = 0.1033; Y27: p = 0.0001; CytoD: p < 1e-4
Fig. 6C	Independent sample values, known reference	One-sample sign test	QNZ: p < 1e-4 ; DAPT: p < 1e-4; Y27: p < 1e-4; CytoD: p < 1e-4
Fig. 6E	Normality, independent sample	One-sample t-test	QNZ: p = 0.0502; DAPT: p = 0.9662; Y27: p = 0.5176;

	values, equal variances, known reference		CytoD: p = 0.1836
Supplementary Fig. 3C	Same as Fig. 3D		
Supplementary Fig. 3D	Normality, independent sample values, equal variances, multiple comparisons	ANOVA, parametric posthoc procedure with Sidak's correction	1 vs 2: p = 1.0000; 2 vs 3: p = 1.0000; 3 vs 4: p = 0.0002; 4 vs 5: p < 1e-4; 5 vs 6: p < 1e-4; 6 vs 7: p < 1e-4; 7 vs 8: p < 1e-4; *v 9: p = 1.0000; 9 vs 10: p < 1e-4
Supplementary Fig. 4A	Independent sample values, known reference	One-sample sign test	DMSO: p = 1.0000; Secondary: p < 1e-4
Supplementary Fig. 7	Independent sample values,	known reference One-sample t-test	QNZ: p = 0.8707; DAPT: p = 0.8133; Y27: p = 0.2687; CytoD: p = 0.1544

SUPPLEMENTARY FIGURES

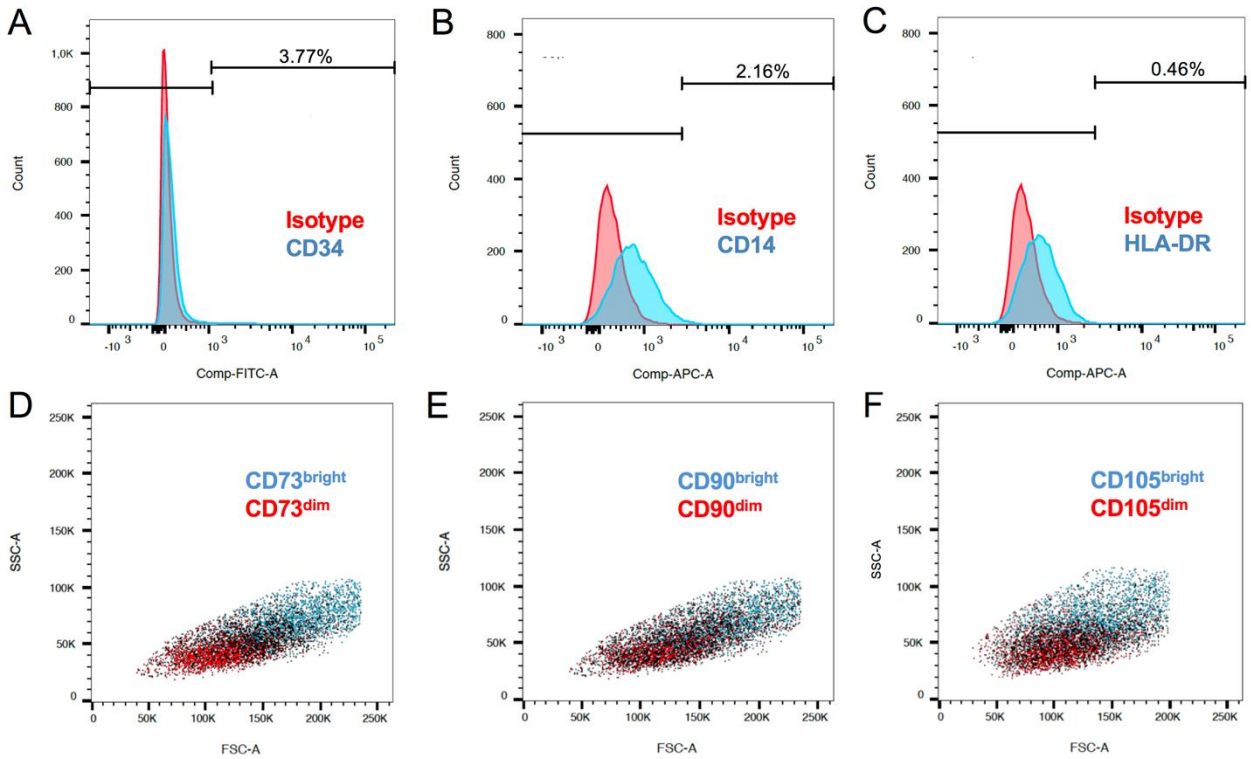

Fig. S1. Characterization of the hMSC population. Representative histograms of the percentage of hMSCs expressing CD34 (**A**), CD14 (**B**) and HLA-DR (**C**). Correlation between cell size (FSC and SSC) and level of CD73 (**D**), CD90 (**E**) and CD105 (**F**) expression.

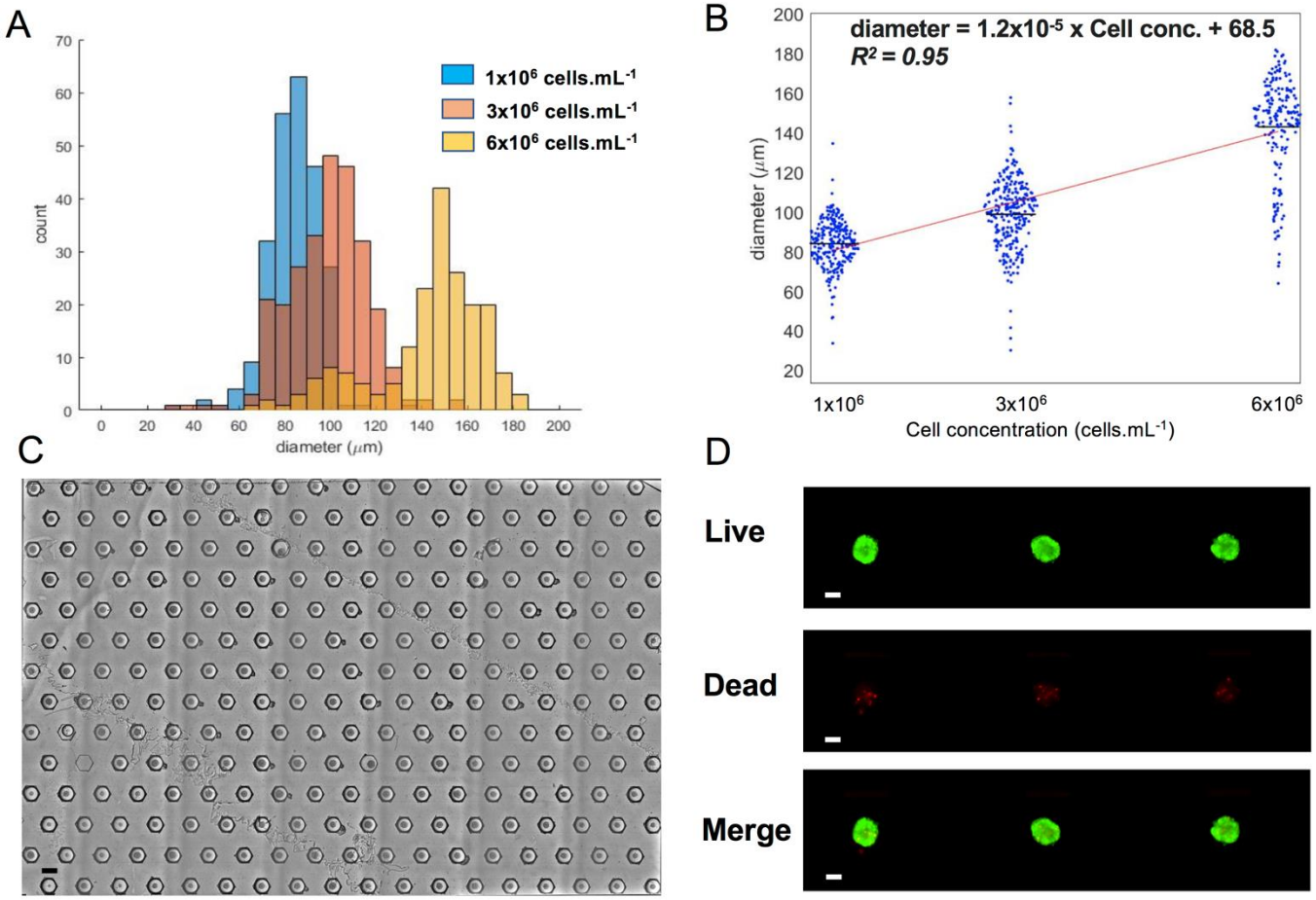

Fig. S2. Formation of MBs on chip. Different hMSC concentrations in the seeding solution yield to the formation of MBs with different sizes that increase with the cell concentration (**A**). There is a linear correlation between the hMSC concentration in the seeding solution and the diameter of the resulting MBs. From the regression curve and considering the monodisperse distribution of the volume of the droplets (50 nL), the average cell number in each droplet is of 380 cells and the C.V. is of 24%. The protocol yields to the formation of just one MBs in each anchor, scale bars are 300 μm (**C**). Live dead imaging of MBs, scale bars are 100 μm (**D**). The images were acquired using a widefield microscope.

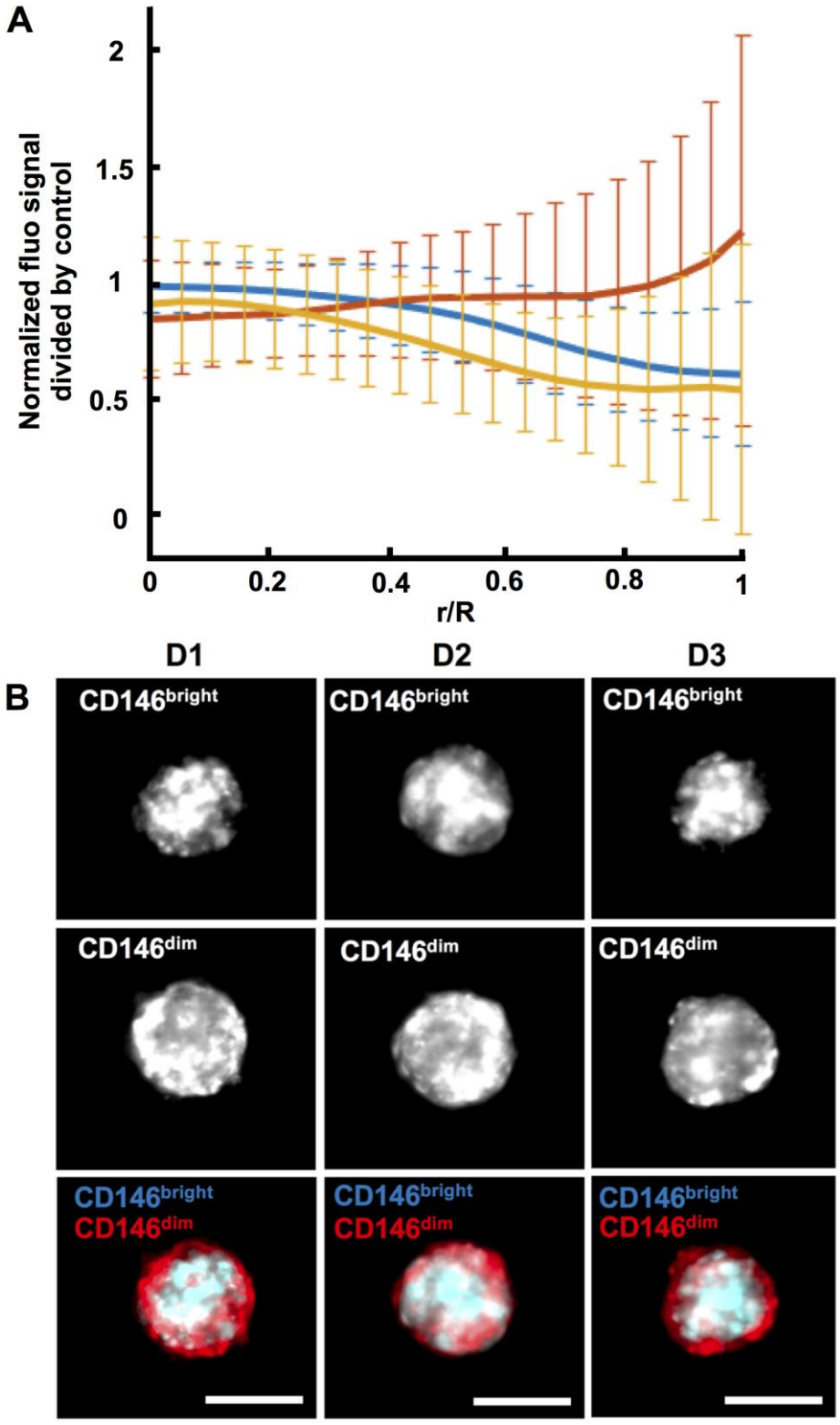

Fig. S3. Structural organization in MBs. Radial coordinates of $CD146^{dim}$ (n_{MBs} = 85, red line), $CD146^{bright}$ (n_{MBs} = 500, blue line) and the larger cells (n_{MBs} = 120, orange line) of the hMSC population in MBs, after Vibrant®DIL staining, error bars represent the standard deviation, the images were acquired using a widefield microscope (**A**). Representative images of the time evolution of the structural organization in MBs from day 1 to day 3 in culture (n_{MBs} = 61) (**B**). Scale bar are 100 μm.

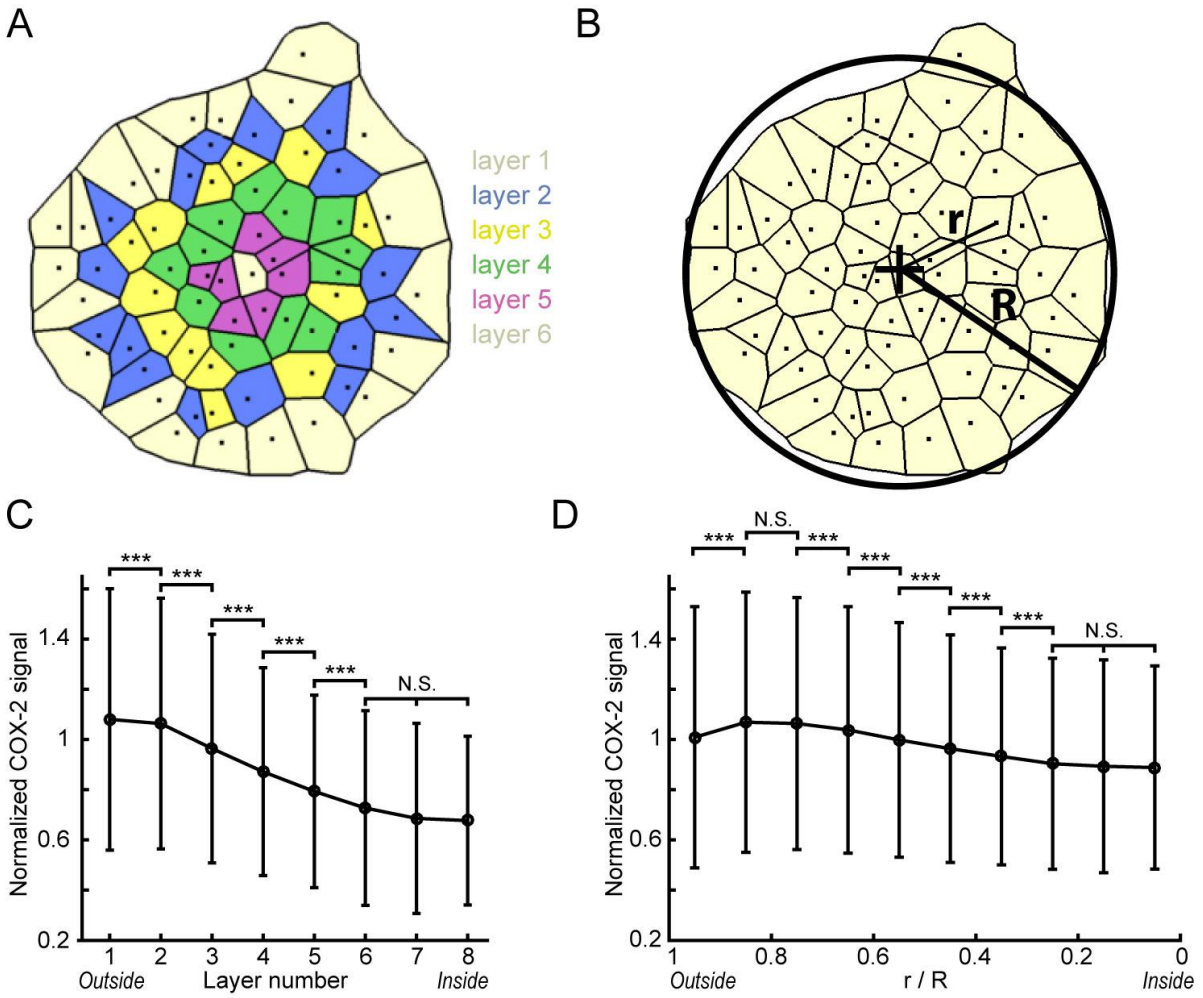

Fig. S4. Intra-MB analysis of the COX-2 signal with concentric cell layers. (**A-B**) Schemes of the same MB where the cell centers are represented by black dots. Black lines show the Voronoi cells. The position of each cell in the MB is described by assigning a cell layer number (A, each color represents a cell layer, layer number 1 being the outermost cell layer) or by computing its normalized distance to the MB center r / R (B, r is the distance between the cell center and the MB center and R is the equivalent radius of the MB). (**C-D**) Evolution of the normalized cellular COX-2 signal with the cell layer number (C) and the normalized distance to the MB center (D). Black circles and errors bars represent respectively the mean normalized COX-2 signal and the standard deviation of the data. N_{chips} = 13; n_{MBs} = 2,936; n_{cells} = 159,596. The layer analysis gives a much clearer trend with a higher COX-2 signal in the layers close to the MB edge, as can be seen in Fig. 5.D-E. The uncertainty of the cell center determination and the fact that two cells of a not perfectly round MB can have different r / R values even if they belong to the same concentric layer explain why the cell layer assignment is a more accurate determination of the cell location in the MB. ***: $p < 0.001$; N.S.: non significant.

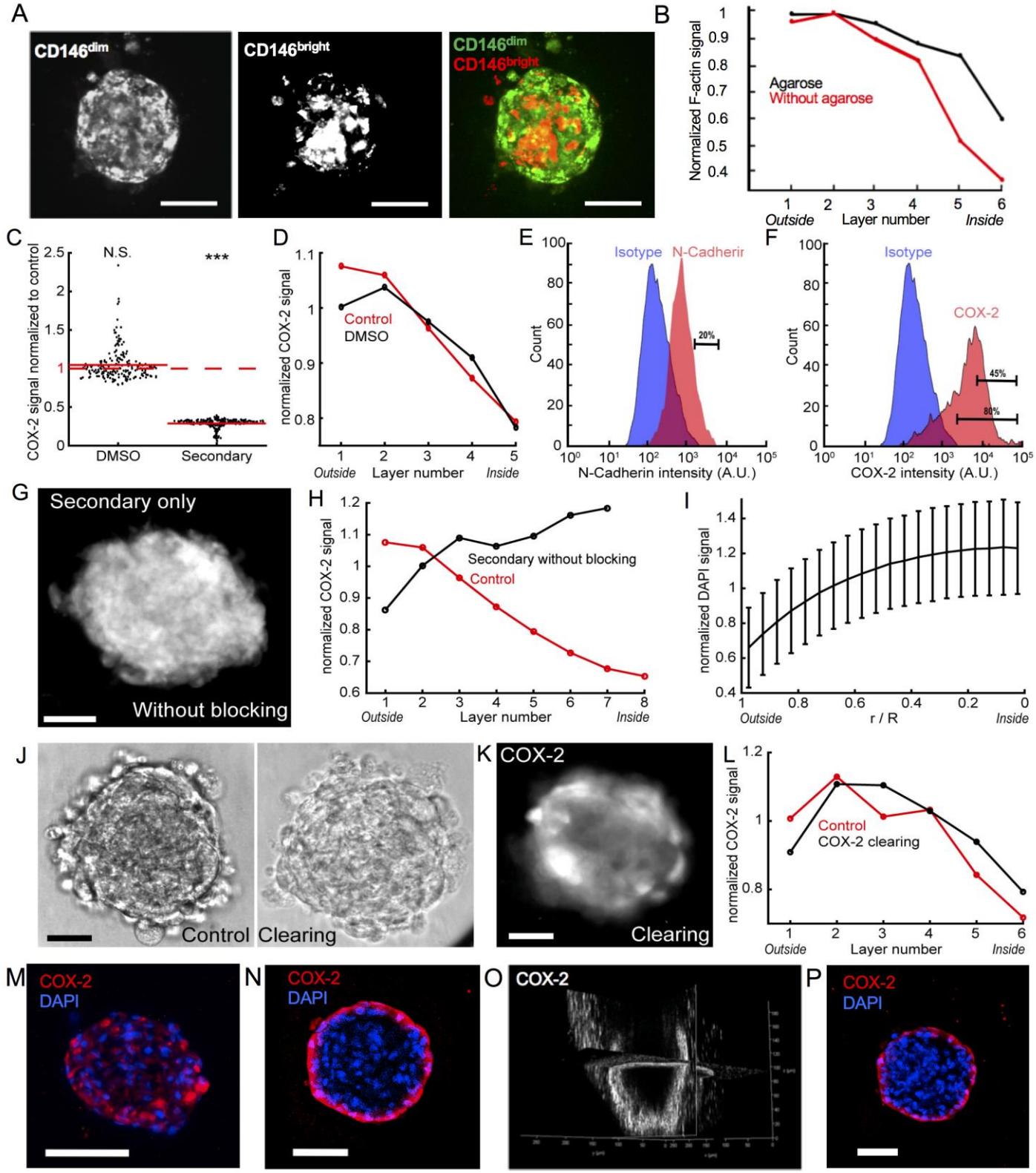

Fig. S5. Validation of the fluorescence signal patterns. Representative images of the median plan of MBs formed with CD146^{dim} and CD146^{bright} stained for Vibrant®DIL and Vibrant®DIO, using a spinning disc-confocal microscope (n_{MBs} = 100) (**A**). Distribution of fluorescent signal of F-actin in the cell layers of MBs cultivated with or without agarose (**B**). (**C-D**) Specificity of the staining and non-interference of the DMSO. Performing the immunostaining without the primary antibody and staining only with secondary antibody resulted in a very low fluorescent signal, which validated the specificity of the primary antibodies (C, control for secondary: N_{chips} = 1;

n_{MBs} = 192; secondary: N_{chips} = 1; n_{MBs} = 251). MBs were formed and cultivated in the presence of 0.1 % (v/v) DMSO (the maximum concentration in culture media containing the inhibitors). Similar average per chip (C, control for DMSO: N_{chips} = 3; n_{MBs} = 644; DMSO 0.1 % (v/v): N_{chips} = 1; n_{MBs} = 195) and distribution of fluorescent signal in the cell layers (D, DMSO 0.1 % (v/v): n_{cells} = 5,982) demonstrated the absence of contribution of 0.1 % (v/v) DMSO in the cell behavior within MBs. (**E**-**F**) Flow cytometry analysis of the percentage of COX-2^{high} (E) and N-cadherin (F) expressing cells, after MBs dissociation and immunostaining, revealed the presence of several subpopulations expressing different levels of these proteins, however, without any spatial information (at least 5000 cells were analysis for each condition). (**G**-**H**) Removing the blocking step during the staining showed that there is no limitation for antibody diffusion. The cells were fixed, permeabilized and then stained only with the secondary antibody, without blocking the samples (G), rendering all immunogenic sites of the MBs accessible. Fluorescent signal distribution in the different cell layers demonstrated higher signal intensity in the core of MBs than in the edge (H, Control: N_{chips} = 13; n_{MBs} = 2,936; n_{cells} = 159,596; Secondary without blocking: N_{chips} = 1; n_{MBs} = 17; n_{cells} = 1,618). (**I**-**K**) Quantifying the DAPI signal (I) and clearing the samples (J-K) showed that there was no significant light path alteration in the 3D MBs. (**L**) The DAPI fluorescent signal distribution inside the MBs displayed a continuous signal increase from the edge (r/R = 1) to the core (r/R = 0; N_{chips} = 55; n_{MBs} = 10,072; n_{cells} = 699,836), which demonstrated that there is no diffusion limitation of small molecules and that the fluorescent light path is not attenuated by the MB opacity. (J-L) The MBs were subjected to ClearT2 treatment after the immunostaining for COX-2. Representative images (J) showed that the MBs were efficiently cleared post ClearT2, but the distribution of the fluorescent signal intensity was not affected, as demonstrated by a representative MB (K) and the quantification of the distribution of the fluorescent signal after clearing in the different cell layers (L, control COX-2: N_{chips} = 1; n_{MBs} = 23; n_{cells} = 2,366; clearing COX-2: N_{chips} = 1; n_{MBs} = 67; n_{cells} = 6,333). The MBs were recovered from the chip then cryosectionned at 7 μm. For this cell layer depth, there is no antibody diffusion limitation or light path alteration. Here again, the intensity of the COX-2 signal is higher at the edges of the MB than in the central region (**M**). Alternatively, the MBs were image using a 2-photons microscope and the COX-2 fluorescent signal pattern show similar distribution as wide field imaging, in the median plan (**N**), cross-section of fluorescence on the x-y and x-z planes (**O**) or maximal z-projection (**P**). All scale bars are 50 μm. These results demonstrated the reliability of the measurements by image analysis, ensuring (1) the specificity of the fluorescent labeling; (2) the absence of limitation for antibody diffusion; (3) the absence of the light path alteration in the 3D structures.

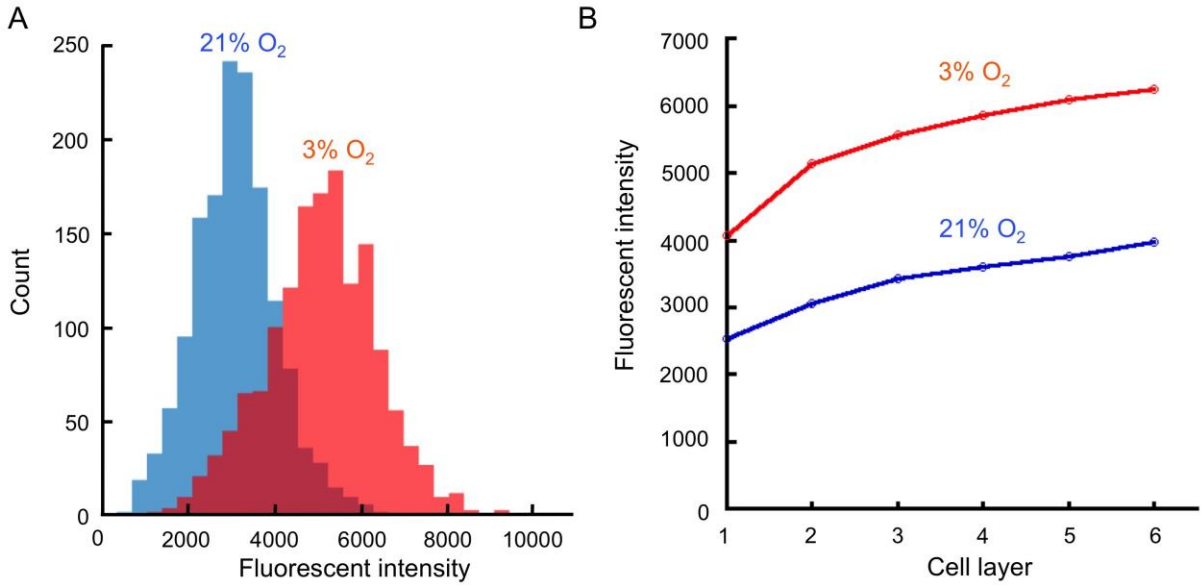

Fig. S6. Hypoxia analysis within MBs. Mesenchymal bodies were incubated with Image-iT™ Red Hypoxia Reagent and placed in incubators set up at 21% or 3% O_2. After 24h, a higher number of cells was positive for Image-iT™ Red Hypoxia Reagent at 3% than at 21% O_2 (**A**). While a slight increase in hypoxia signal was detected in the inner cell layers at 21%O_2, this fluorescent signal never reached the level measured at 3% O_2, even in the most outer layers (**B**), demonstrating the absence of hypoxic core in the MBs. The images were acquired using a widefield microscope

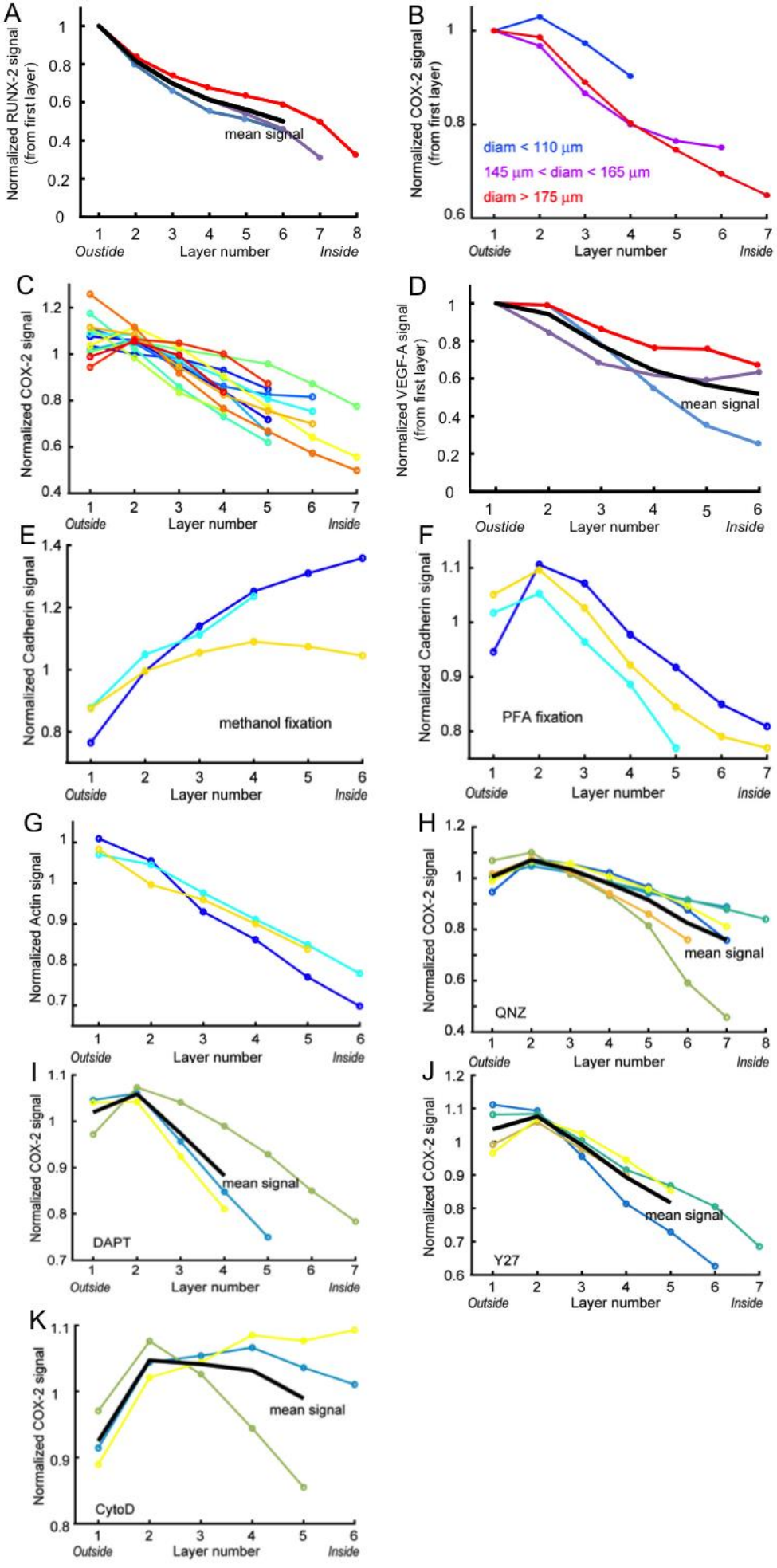
A
Normalized RUNX-2 signal (from first layer)
mean signal
Oustide
Layer number
Inside
B
Normalized COX-2 signal (from first layer)
diam < 110 μm
145 μm < diam < 165 μm
diam > 175 μm
Outside
Layer number
Inside
C
Normalized COX-2 signal
Outside
Layer number
Inside
D
Normalized VEGF-A signal (from first layer)
mean signal
Oustide
Layer number
Inside
E
Normalized Cadherin signal
methanol fixation
Outside
Layer number
Inside
F
Normalized Cadherin signal
PFA fixation
Outside
Layer number
Inside
G
Normalized Actin signal
Outside
Layer number
Inside
H
Normalized COX-2 signal
mean signal
QNZ
Outside
Layer number
Inside
I
Normalized COX-2 signal
mean signal
DAPT
Outside
Layer number
Inside
J
Normalized COX-2 signal
mean signal
Y27
Outside
Layer number
Inside
K
Normalized COX-2 signal
mean signal
CytoD
Outside
Layer number
Inside

Fig. S7. Intra-MB fluorescence signal distribution in individual chip. Evolution of the intra-MB fluorescent signal with control conditions. (**A**) Normalized mean RUNX-2 with the cell layer number, (**B**) Normalized mean COX-2 with the cell layer number for MBs having different sizes (N_{chips} = 13; blue, diameter < 110 μm, n_{MBs} = 298, n_{cells} = 9,282; purple, 145 μm< diameter < 165 μm, n_{MBs} = 620, n_{cells} = 42,469; red, diameter > 175 μm, n_{MBs} = 295, n_{cells} = 26,251) in control conditions. (**C**) Normalized mean COX-2 (C, N_{chips} = 13, n_{MBs} = 2,936, n_{cells} = 159,596), (**D**) Normalized mean VEGF-A (N_{chips} = 3, n_{MBs} = 413), cadherin (**E**, with methanol fixation, N_{chips} = 3, n_{MBs} = 405, n_{cells} = 24,185; **F**, with PFA fixation, N_{chips} = 3, n_{MBs} = 649, n_{cells} = 47,254) and actin (**G**, N_{chips} = 3, n_{MBs} = 421, n_{cells} = 23,970) signals with the cell layer number. Each color represents the mean behavior for one chip. (**H**-**K**) Evolution of the normalized mean COX-2 signal with the cell layer number depending on the inhibitor: QNZ (H, N_{chips} = 6, n_{MBs} = 1,215, n_{cells} = 117,443), DAPT (I, N_{chips} = 3, n_{MBs} = 658, n_{cells} = 37,165), Y27 (J, N_{chips} = 4, n_{MBs} = 709, n_{cells} = 45,839) or CytoD (K, N_{chips} = 3, n_{MBs} = 458, n_{cells} = 28,981). Each color represents the mean behavior for one chip. The black lines represent the mean of the single chips. All the images were acquired using a widefield microscope

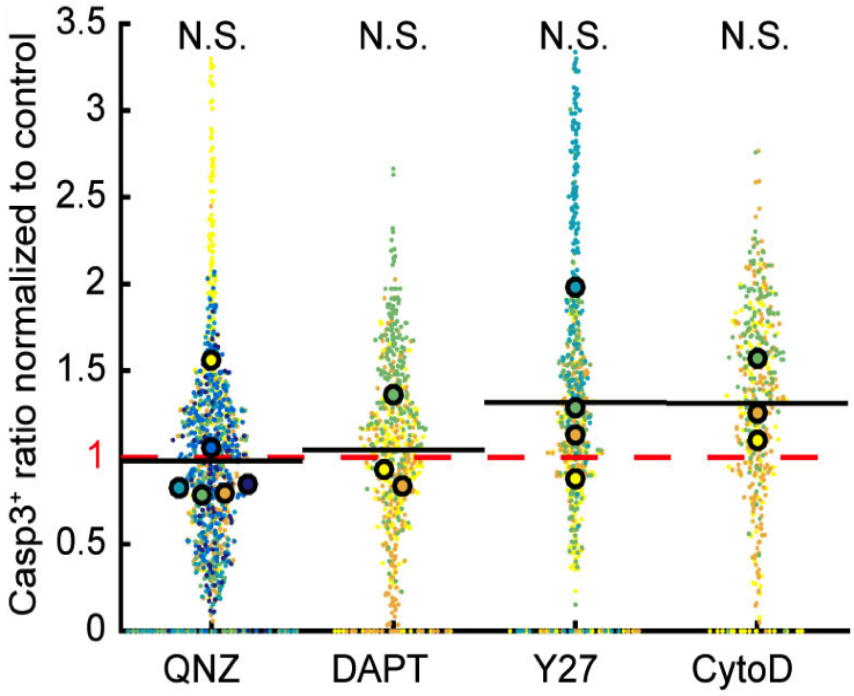

Fig. S8. Ratio of Casp3$^+$ cells per MB formed with QNZ (n_{MBs} = 1216), DAPT (n_{MBs} = 658), Y27 (n_{MBs} = 709), and CytoD (n_{MBs} = 458). For each of these experiments, the results are normalized by the mean of the corresponding control. N.S.: not significant; **: $p < 0.01$. The images were acquired using a widefield microscope